Supporting Information

Wang et al. 10.1073/pnas.1112129109

SI Materials and Methods

Plasmids. Mammalian expression plasmids encoding HA-von Hippel–Lindau (VHL)(WT), HA-hypoxia-induced factor (HIF)1α, HA-HIF1α(P564A), and HA-HIF2α were described previously (1). A plasmid encoding caveolin 1 (CAV1) was generously provided by Jeff Pessin (Albert Einstein College of Medicine, New York). pcDNA3-HA-HIF2α(P531A) was generated using the QuikChange Site-Directed Mutagenesis kit (Stratagene) using pcDNA3-HA-HIF2α as a template and the following primers: 5′-GGAGACACTGGCAGCCTATATCCCCATGG-3′ and 5′-CCATGGGGATATAGGCTGCCAGTGTCTCC-3′. The integrity of the plasmid was verified by direct DNA sequencing.

Antibodies and Ligands. Monoclonal anti-HA (12CA5) antibody was obtained from Roche Molecular Biochemicals. Anti-EGF receptor (EGFR) (1005), anti–phospho-ERK(Tyr204), and anti–phospho-tyrosine (PY99) antibodies were obtained from Santa Cruz. Anti–α-tubulin antibody was obtained from Sigma-Aldrich. Anti–HIF1α, anti-HIF2α, and anti-carbonic anhydrase IX antibodies were obtained from Novus Biologicals Inc. Anti-VHL (IG32) antibody was obtained from BD Transduction Laboratories. Polyclonal and monoclonal anti-CAV1 and anti-glucose transporter type 1 (GLUT1) antibodies were obtained from Abcam. Anti-PDGF receptor (PDGFR), anti–phospho-PDGFR (Tyr751), anti–phospho-insulin-like growth factor type 1 receptor (IGF1R) (Tyr1131), anti–phospho-Akt (Ser473), anti-Akt, anti–phospho-A-Raf (Ser299), anti–phospho-B-Raf (Ser455), anti–phospho-C-Raf (Ser388), anti–A-Raf, anti–B-Raf, anti–C-Raf, anti–phospho-MEK(Ser217/221), and anti-MEK antibodies were obtained from Cell Signaling. Anti–phospho-EGF receptor (EGFR) (Tyr845) was obtained from Millipore. EGF was obtained from Sigma-Aldrich and was used at a final concentration of 20 ng mL^{-1}.

Gene Expression Analysis. Gene expression profiles from 10 clear-cell renal cell carcinomas (CCRCC), 13 papillary renal cell carcinomas (RCC), and 12 nondiseased kidney tissue samples were analyzed using the Affymetrix HG-U133 Plus 2.0 GeneChip platform as previously described (2) and were deposited at the Gene Expression Omnibus (accession number GDS1344). These kidney tissue samples were obtained from the Cooperative Human Tissue Network, and internal review board approval was obtained from the Van Andel Research Institute, Grand Rapids, MI. The box-whisker plot (Fig. 1*B* and Fig. S1*C*) was generated using a GraphPad PRISM 5.0 software, and the heat map was generated using Java Treeview software v1.16.

Immunoprecipitation and Immunoblotting. Immunoprecipitation and immunoblotting were performed as previously described (3).

Immunohistochemical Staining. Sample preparation and immunohistochemical staining were performed as described previously (4).

Quantitative Real-Time PCR. Quantitative real-time PCR was performed as previously described (3). Primers sequences are as follows: *CAV1* (5′-TTCGCCATTCTCTCTTTCCT-3′ and 5′-CAGCTTCAAAGAGTGGGTCA-3′); *VEGF* (5′-GCAGACCAAAGAAAGATAGACCAAG-3′ and 5′-CGCCTCGGCTTGTCACAT-3′).

RNAi Knockdown. siGENOME SMARTpool targeted to *VHL*, *CAV1*, and nontargeting scrambled siRNA duplex (5′-CCAUUCCGAUCCUGAUCCG-3′) were obtained from Dharmacon. shRNA targeted to *CAV1, HIF2α*, and nontargeting scrambled shRNA were obtained from Santa Cruz. The transfection of siRNA and shRNA was performed using XtremeGene siRNA Transfection Reagent (Roche) or Fugene 6 Transfection Reagent (Roche) following the manufacturer's protocol.

Chemical Cross-Linking. Monolayer cells were washed five times with ice-cold PBS and were chemically cross-linked for 1 h at 4 °C with freshly prepared 2.5 mM bis(sulfosuccinimidyl) suberate (BS3) (Pierce). To terminate the reaction, cells were incubated with 10 mM Tris (pH 7.5) for 15 min on ice.

DNA Synthesis Assay. DNA synthesis was assayed using the BrdU incorporation kit (Roche) following the manufacturer's instructions. BrdU-positive nuclei were quantified using Image J software (National Institutes of Health).

Transmission Electron Microscopy. Cell pellets were resuspended in a 2% (vol/vol) agarose solution and fixed with glutaraldehyde followed by *en bloc* fixation with 2% (vol/vol) uranyl acetate, fixed in osmium tetroxide, dehydrated by alcohol gradient, and then infiltrated with Spurr's resin. Transmission electron micrographs of these samples were acquired with a TEM-7000 instrument (Hitachi High Technologies America). For quantitation of caveolae, only distinctly flask-shaped, noncoated vesicles (50 nm in diameter) found on the plasma membranes were scored as caveolae. Total caveolae counts were normalized to the unit length of plasma membrane (10 μm) and measured using Image J software.

Fluorescence Microscopy. Cells grown on glass coverslips were fixed by methanol and permeabilized with 0.2% Triton X-100. Next, the cells were incubated for 1 h at room temperature with the indicated primary antibodies followed by incubation with fluorescence-labeled secondary antibodies for 1 h. The immunostained cells were visualized with an Axioplan2 Imaging (Carl Zeiss) microscope in Apotome mode for high optical resolution or with a spinning disk confocal microscope (Quorum Technologies). To verify colocalization, Pearson's correlation coefficient and the resulting colocalization images of the positive product of the differences from the mean (PDM) values were determined using Image J software version 1.40 with Intensity Correlation Analysis plug-in as previously described (5). Notably, Pearson's correlation coefficient ranges from −1 to +1 where 1 represents perfect correlation, −1 represents perfect exclusion, and 0 represents random localization. The PDM value is expressed as PDM = (red intensity − mean red intensity) × (green intensity − mean green intensity), and positive PDM values indicate the presence of colocalization (6).

Wound-Healing Assay. HeLa-shSCR and HeLa-shSCAV1 cells were counted and plated at 1×10^6 cells/mL in six-well dishes to achieve confluency overnight. Wounds were made using a pipette tip, reference points were created using a 20-G 1-in needle (Becton Dickinson), and photographs were taken immediately (time 0) and 16 h after wounding using an inverted Nikon Eclipse TE200 microscope. Cell migration or the extent of wound closure was measured at the reference point. Experiments were carried out in triplicate and were repeated at least three times.

Matrigel Invasion Assay. HeLa-shSCR and HeLa-shSCAV1 cells (1×10^4) were plated in medium without serum or growth factors in the upper chamber of 24-well Transwell (pore size, 8 μm; BD Biosciences) with Matrigel-coated membrane. In the lower chamber, medium supplemented with serum was used as a che-

moattractant. The cells were incubated for 48 h. Cells that did not pass through the pores were removed by a cotton swab.

Cells on the lower surface of the membrane were stained with the Diff-Quick Staining Set (VWR) and counted using an Axioplan2 Imaging microscope (Carl Zeiss). The experiment was repeated in triplicate.

EMSA. The EMSA was performed as previously described (3). The oligos for HRE are as follows: *CAV1* HRE (5′-CCGGCGCAGCACACGTCCGGGCCAA-3′) and *VEGF* HRE (5′-CACAGTGCATACGTGGGCTCCAAC-3′).

ChIP. The ChIP assay for Pol II was performed as described previously using the Upstate ChIP assay kit (7). The ChIP assays for HIF1α and HIF2α were performed as previously described (8) with anti-HIF1α (Abcam) and anti-HIF2α (Novus Biological) rabbit polyclonal antibodies according to the manufacturer's instructions. Primer sequences for the promoter of human *CAV1* are as follows: CAV1-F, 5′-AACGTTCTCACTCGCTCTCTG-3′ and CAV1-R, 5′-GCCAAAGGTTTGTTCTGCTC-3′. The annealing temperature was 60 °C. The primer sequences for the promoter of human *Gapdh* were as previously described (8).

Mouse Dorsal Skin-Fold Window Chamber Assay. All animal experiments were performed in accordance with the institutional animal care guidelines (University Health Network, Toronto, ON, Canada). The mouse dorsal window chamber assay was performed as described previously (9).

Statistical Methods. A two-tailed Welch's *t* test was used to determine differences in gene expression. A Mann–Whitney test was used to compare the tumor growth determined by bioluminescence imaging. An unpaired two-tailed Student's *t* test was used to compare the other two treatment groups. A one-way ANOVA followed by a Newman–Keuls post hoc test was performed to compare multiple treatment groups. All statistical analysis was performed using GraphPad PRISM 5.0 software. Statistical significance was achieved at $P < 0.05$. All results are representative of at least three independent experiments.

1. Lonergan KM, et al. (1998) Regulation of hypoxia-inducible mRNAs by the von Hippel-Lindau tumor suppressor protein requires binding to complexes containing elongins B/C and Cul2. *Mol Cell Biol* 18:732–741.
2. Yang XJ, et al. (2005) A molecular classification of papillary renal cell carcinoma. *Cancer Res* 65:5628–5637.
3. Wang Y, et al. (2009) Regulation of endocytosis via the oxygen-sensing pathway. *Nat Med* 15:319–324.
4. Evans AJ, et al. (2007) VHL promotes E2 box-dependent E-cadherin transcription by HIF-mediated regulation of SIP1 and snail. *Mol Cell Biol* 27:157–169.
5. French AP, Mills S, Swarup R, Bennett MJ, Pridmore TP (2008) Colocalization of fluorescent markers in confocal microscope images of plant cells. *Nat Protoc* 3:619–628.
6. Varecha M, et al. (2007) Bioinformatic and image analyses of the cellular localization of the apoptotic proteins endonuclease G, AIF, and AMID during apoptosis in human cells. *Apoptosis* 12:1155–1171.
7. Fish JE, et al. (2005) The expression of endothelial nitric-oxide synthase is controlled by a cell-specific histone code. *J Biol Chem* 280:24824–24838.
8. Chung J, et al. (2010) SATB2 augments ΔNp63α in head and neck squamous cell carcinoma. *EMBO Rep* 11:777–783.
9. Sufan RI, et al. (2009) Oxygen-independent degradation of HIF-alpha via bioengineered VHL tumour suppressor complex. *EMBO Mol Med* 1:66–78.

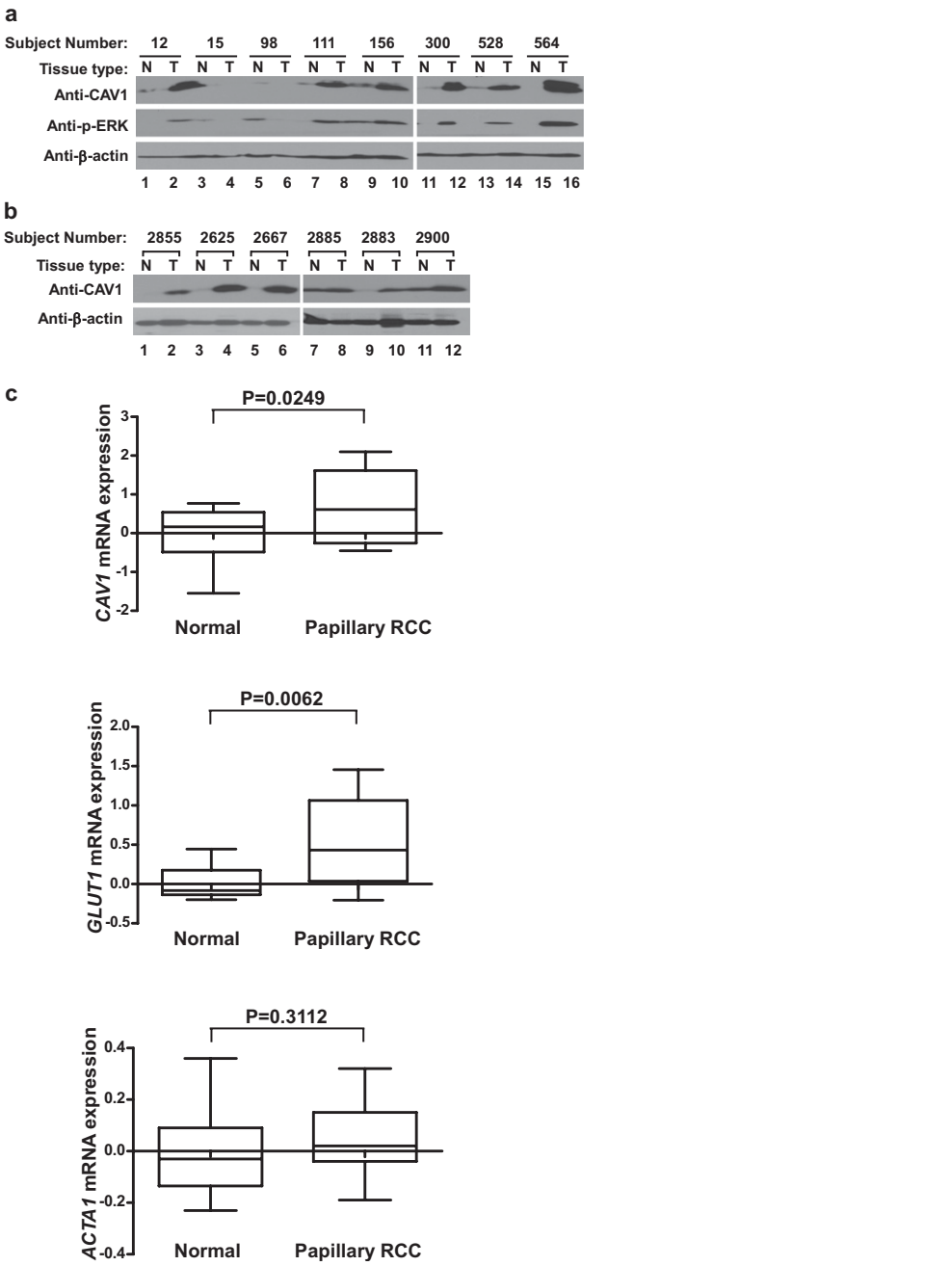

Fig. S1. RCC samples with a strong hypoxic signature display increased CAV1 mRNA and protein levels. (*A*) Cellular extracts generated from primary CCRCC (T) and matched normal (N) kidney samples were resolved by SDS/PAGE and immunoblotted with the indicated antibodies. (*B*) Cellular extracts generated from primary papillary RCC and matched normal kidney samples were separated by SDS/PAGE and immunoblotted with the indicated antibodies. (*C*) Relative gene expression levels of *CAV1*, *GLUT1*, and *ACTA1* (encoding α-actin, negative control) in papillary RCC ($n = 10$) and nondiseased kidney (normal; $n = 11$) are shown as a box and whisker plot. Whiskers indicate 0% and 100% quartiles; the boxes indicate the 25% and 75% quartiles; the horizontal lines within the boxes indicate the 50% quartiles. *P* value was calculated by using a two-sided Welch's *t* test.

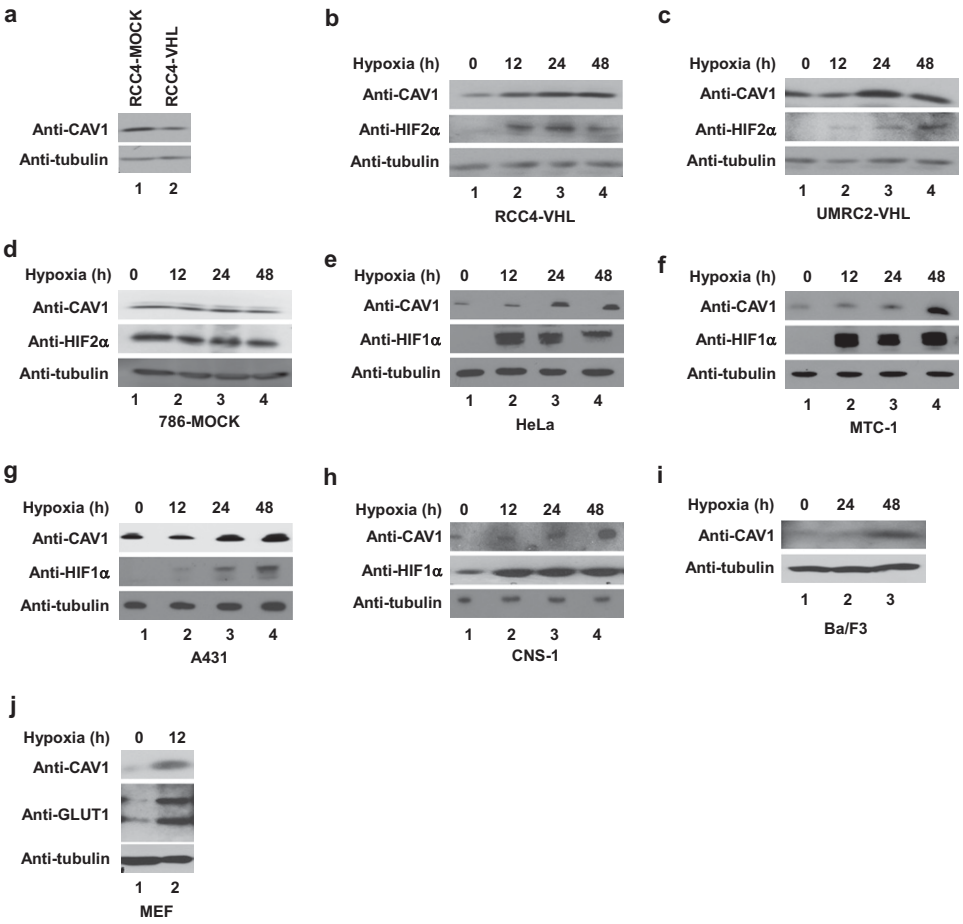

Fig. S2. Hypoxia regulates CAV1 expression. (*A*) Total cell lysates of RCC4-MOCK and RCC4-VHL cells were resolved by SDS/PAGE and immunoblotted with the indicated antibodies. (*B–J*) The indicated cell lines and primary mouse embryonic fibroblasts were maintained in hypoxia for the indicated times. Equal amounts of total cell lysates were separated by SDS/PAGE and immunoblotted with the indicated antibodies.

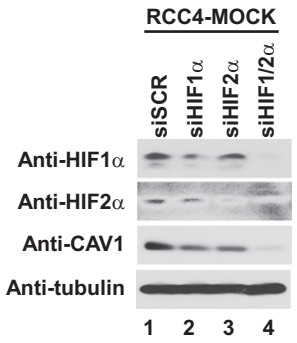

Fig. S3. Knockdown of HIF down-regulates CAV1 expression. HIF1α and/or HIF2α were specifically knocked down by siRNA in RCC4-MOCK cells. Equal amounts of total cell lysates were separated by SDS/PAGE and immunoblotted with the indicated antibodies.

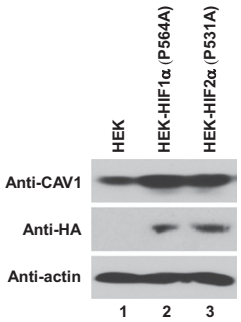

Fig. S4. HIF up-regulates CAV1 expression. HEK-293 cells were transfected with plasmids encoding HA-HIF1α(P564A) or HA-HIF2α(P531A). Equal amounts of total cell lysates were separated by SDS/PAGE and immunoblotted with the indicated antibodies.

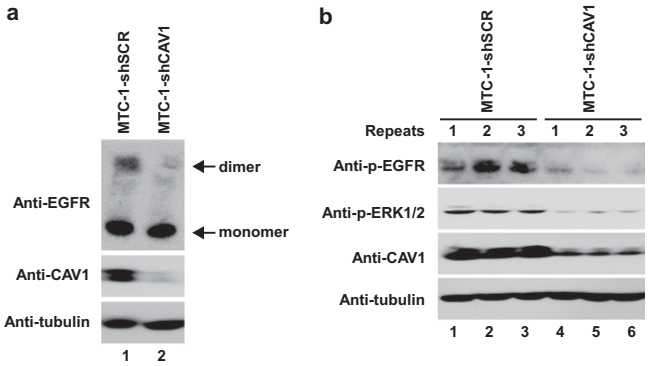

Fig. S5. CAV1 promotes ligand-independent EGFR dimerization and phosphorylation in MTC-1 cells. (*A*) Equal amounts of total cell lysates generated from serum-starved and chemically cross-linked MTC-1-shSCR and MTC-1-shCAV1 cells were resolved by SDS/PAGE and immunoblotted with the indicated antibodies. (*B*) MTC-1-shSCR and MTC-1-shCAV1 cells were serum starved overnight, and equal amounts of total cell lysates were separated by SDS/PAGE and immunoblotted with the indicated antibodies.

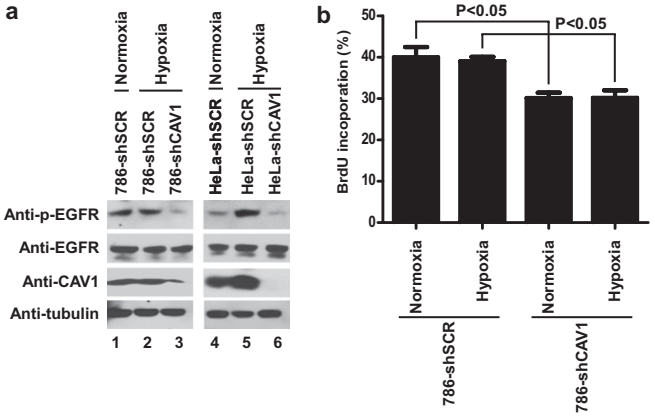

Fig. S6. Knockdown of CAV1 inhibits HIF-mediated ligand-independent EGFR phosphorylation and cell proliferation in 786-O and HeLa cells. (*A*) Serum-starved 786-shSCR, 786-shCAV1, HeLa-shSCR, and HeLa-shCAV1 cells were maintained in hypoxia or normoxia for 24 h. Equal amounts of total cell lysates were separated by SDS/PAGE and immunoblotted with the indicated antibodies. (*B*) BrdU incorporation by 786-shSCR and 786-shCAV1 cells was measured following serum starvation with or without hypoxia treatment for 24 h. Values indicate the mean percentage of BrdU-positive cells in relation to total DAPI-stained nuclei from three independent experiments. Error bars indicate SD. *P* values were calculated using the Newman–Keuls post hoc test.

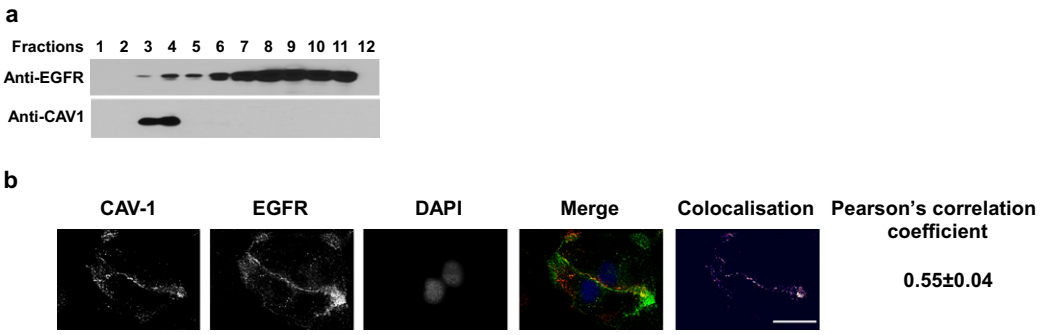

Fig. S7. CAV1 and EGFR partially colocalize in the absence of ligand. (*A*) Serum-starved 786-O cells were subjected to subcellular fractionation on a sucrose gradient into 12 continuous fractions after homogenization. Fractions then were resolved by SDS/PAGE and immunoblotted with the indicated antibodies. (*B*) Serum-starved 786-O cells were immunostained with anti-CAV1 polyclonal and anti-EGFR monoclonal antibodies followed by secondary Alexa 488 anti-rabbit (green) and Rhodamine anti-mouse (red) antibodies, respectively. The resulting colocalization images of the positive PDM values and the Pearson correlation coefficient were determined using Image J software version 1.40. (Scale bar: 5 μm.)

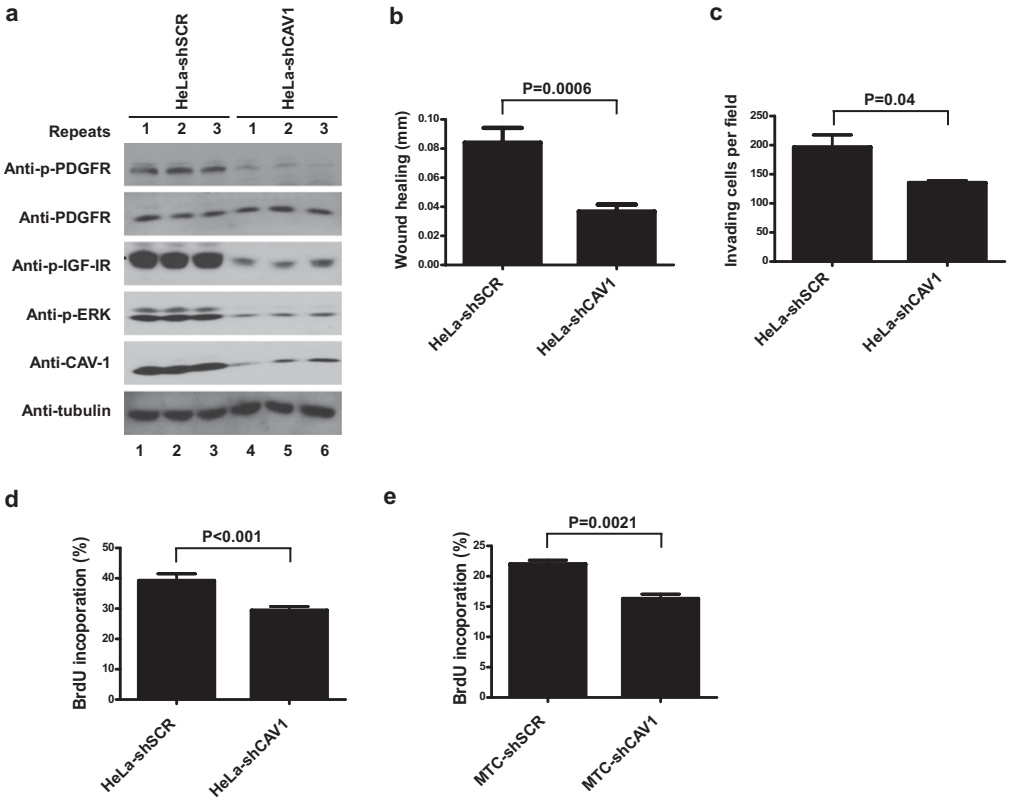

Fig. S8. CAV1 promotes cell proliferation and ligand-independent activation of other receptor tyrosine kinases. (*A*) HeLa-shSCR and HeLa-shCAV1 cells were serum starved overnight, and equal amounts of total cell lysates separated by SDS/PAGE were immunoblotted with the indicated antibodies. (*B* and *C*) The wound-healing (*B*) and Matrigel invasion (*C*) assays of HeLa-shSCR and HeLa-shCAV1 cells were performed as described in *SI Materials and Methods*. Error bars represent SD. *P* values were calculated using Student's *t* test. (*D* and *E*) BrdU incorporation by HeLa-shSCR and HeLa-shCAV1 cells (*D*) and by MTC-shSCR and MTC-shCAV1 cells (*E*) was measured following serum starvation for 16 h under hypoxia. Values indicate the mean percentage of BrdU-positive cells in relation to total DAPI-stained nuclei from three independent experiments. Error bars indicate SD. *P* values were calculated using the unpaired two-tailed Student's *t* test.

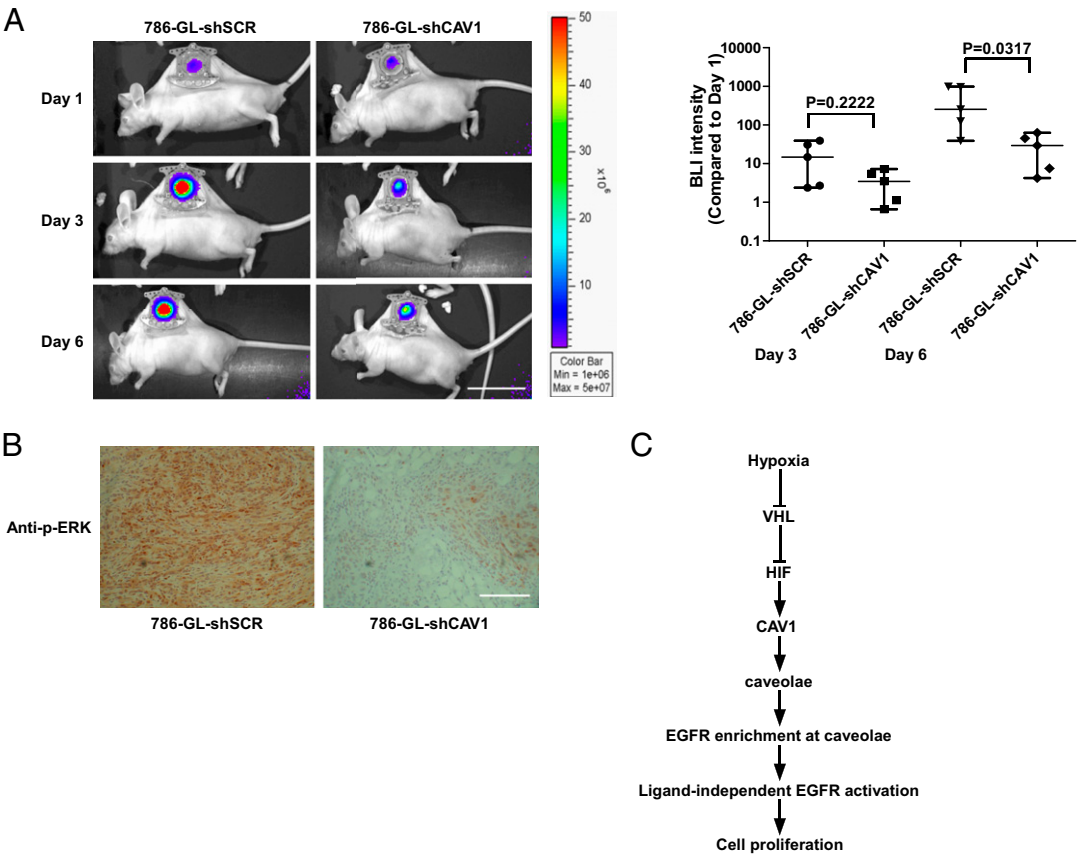

Fig. S9. CAV1 knockdown suppresses CCRCC xenograft growth in mice. 786-GL-shSCR or 786-GL-shCAV1 cells were implanted into the dorsal skin-folds within the window chambers in SCID mice. (*A*) Tumor xenografts were visualized by BLI on days 1, 3, and 6. Representative images (*Left*) and a scatter plot (*Right*) are shown ($n = 5$ for each group) (Scale bar: 10 mm.). (The BLI intensity at day 1 was set arbitrarily at 1. Whiskers indicate the range of the data set, and the middle line indicates the median. Individual animals are indicated on the graph by circles, squares, or diamonds. *P* values were calculated using a Mann–Whitney test. (*B*) Tumors were resected and immunostained with anti–phospho-ERK antibody. (Scale bar: 100 μm.) (C) Model of hypoxia-driven CAV1-mediated EGFR signaling.